ISSN: 3092-8729 | e-ISSN: 3092-8737

ACJPAS

https://acjpas.acu.edu.ng

VOL. 5, NO. 1 2026

Ajayi Crowther Journal of Pure and Applied Sciences

DOI: https://doi.org/10.56534/acjpas.v5i1

A publication of the Faculty of Natural Sciences, Ajayi Crowther University

ISSN: 3092-8729 | e-ISSN: 3092-8737

Ajayi Crowther Journal of Pure and Applied Sciences
https://acjpas.acu.edu.ng

Ajayi Crowther J. Pure Appl. Sci. 2026, 5(1), 11-27.
https://doi.org/10.56534/acjpas.2026.v5.i1.193

Article

Numerical Investigation of Turbulent Convective Heat Transfer of Distilled Water Flowing in Corrugated Converging Pipes

Taiwo Bukola Fasiku[1*], Adebimpe Amos Amosun[2] and Ayobami Jeremiah Awodunmila[2]

[1]Department of Physics, Faculty of Natural Sciences, Ajayi Crowther University, Oyo, Nigeria; (T.B.F.)

[2]Center for Energy and Research Development, Obafemi Awolowo University, Ile-Ife, Nigeria; bimamosun@gmail.com (A.A.A), awodumilaayobami@gmail.com (A.J.A.)

*Corresponding Author: T. B. Fasiku (ayenitaiwobukola@gmail.com)

Article history: *Received: Jan. 6, 2026, Revised: Mar. 3, 2026, Accepted: Mar. 3, 2026, Published: Mar. 17, 2026.*

Abstract

This study examined the turbulent heat transfer performance, the Poiseuille number, and the performance evaluation criterion (PEC) of distilled water flowing in corrugated converging pipes. It systematically investigated the effects of the amplitude of the corrugation ($0.02 \leq e/D \leq 0.03$) and the Reynolds number ($0.5 \times 10^4 \leq Re \leq 4.0 \times 10^4$) on both thermal and flow fields. The governing equations and boundary conditions were numerically solved using the Shear Stress Transport (SST) turbulence model. The results indicated that as the corrugation amplitude increased, the average Nusselt number (Nu), the normalised average Nusselt number (Nu^G), the Poiseuille number (fRe), the normalised Poiseuille number (fRe^G), and PEC increased. At $Re = 4.0 \times 10^4$, $DR = 1.2$, $\frac{w}{D} = 0.2$ and $\frac{e}{D} = (0.02, 0.025 \,\&\, 0.03)$, the average Nusselt numbers were 348.48, 360.69 and 368.78, respectively. The corresponding fRe values were 4407.89, 4502.67, and 4571.15, respectively. The Nu^G values at $Re = 1.5 \times 10^4$ for $e/D = 0.02, 0.025 \,\&\, 0.03$ were 1.36, 1.46 and 1.52, respectively. The fRe^G values at $Re = 3.0 \times 10^4$ for e/D (0.02, 0.025, and 0.03) were 3.16, 3.22 and 3.27, respectively. The corrugated converging pipe enhanced Nu compared with a smooth pipe for all the pipe configurations considered, as revealed by $Nu^G > 1$.

Keywords: Poiseuille number, Nusselt number, Enhancement, Boundary equations, Corrugation amplitude.

Nomenclature

e/D	Corrugation amplitude
w/D	Corrugation width
C_p	Specific heat capacity at constant pressure $[J\ kg^{-1}K^{-1}]$
Nu	Nusselt number
Re	Reynolds number
fRe	Poiseuille number
Pr_t	turbulent Prandtl number
Be	Bejan number
fRe^G	Normalised Poiseuille number
Nu^G	Normalised average Nusselt number
ω	Specific dissipation rate $[\ kgm^{-1}s^{-1}]$
k	Turbulent kinetic energy $[m^2\ s^{-2}]$

q''	Heat flux $[W\ m^{-2}]$
dP	Pressure drop $[Nm^{-2}]$
y^+	Non-dimensional wall parameter of distance
Y_k	Turbulent dissipation of k $[J\ kg^{-1}]$
G_k	Rate of production of k $[J\ kg^{-1}]$
λ	Thermal conductivity $[W\ m^{-2}\ K^{-1}]$
Γ_k	Effective diffusion of k $[kg\ m^{-1}\ s^{-1}]$
Γ_ω	Effective diffusion of ω $[kg\ m^{-1}\ s^{-1}]$
G_k	Generation of turbulent kinetic of k $[kg\ m^{-1}\ s^{-1}]$
G_ω	Generation of turbulent kinetic of ω $[kg\ m^{-1}\ s^{-1}]$
ρ	Density $[kg\ m^{-3}]$
D	Tube diameter $[m]$
μ_t	Turbulent viscosity $[kg\ m^{-1}\ s^{-1}]$
ϵ	Eddy dissipation rate $[m^2\ s^{-3}kg]$

Abbreviations

CHTP	Convective heat transfer performance
PEC	Performance evaluation criterion
TBL	Thermal boundary layer
DR	Diameter Ratio
RANS	Reynolds average navier stokes equation

1. Introduction

In recent years, the rapid rise in energy demand has overwhelmed existing systems, highlighting the need for more studies on energy management. Heat exchangers are essential equipment to ensure heat transfer between media at specified rates and temperatures. Among energy transfer systems, they have played a vital role to date. Numerous studies have reported that the material and structure of heat exchanger tubes significantly affect thermal performance (Li *et al*., 2023; Shuvo *et al*., 2023; Abbas and Dhaidan, 2018). Heat exchangers are used in both domestic and industrial applications, such as heating, ventilation, and air conditioning (HVAC), steam condensation for power plants, food industries, chemical plants, and natural gas processing (Zhong *et al*., 2024). The most common type is the smooth pipe heat exchanger, which is widely used in evaporators due to its simple design, ease of manufacture, and cost-effectiveness (Liu *et al*., 2024). However, it is limited by low thermal efficiency. Consequently, research continues to focus on designing more efficient heat exchangers that are also lighter and smaller.

Improvements in convective heat transfer are achieved through three types of enhancement techniques: passive, active, and compound methods (Liao *et al*., 2021). Active methods require a continuous power supply and include surface disturbance, jet impingement, magnetic field-assisted fluid flow, mechanical aids, and vibration (Corcoles *et al*., 2020). Passive methods do not need external power; instead, they involve modifying the tube geometry to increase turbulence and disrupt the boundary layer. Examples include coiled tubes, porous surfaces, surface roughness, dimpled tubes, surface tension devices, corrugated pipes, and converging pipes (Chaurasiya *et al*., 2023). Passive techniques have demonstrated excellent performance due to their simple construction and energy efficiency (Calomino *et al*., 2018; Zhang *et al*., 2021; Peng *et al*., 2025). Compound techniques combine active and passive methods, or different passive techniques, to enhance heat transfer performance (Qin *et al*., 2020). Examples include extended surfaces and surface vibration, roughened surfaces with fluid vibration, ribs with tube inclination, surfactants with extended surfaces, converging pipes with corrugation, and modified pipes with nanofluids (Al-Daamee and Hamza, 2024).

Among these modifications, corrugated surfaces have emerged as one of the most effective passive strategies for maximising heat transfer and overall efficiency, despite the associated increase in pressure drop. The grooves on their walls induce flow disturbance and turbulence, which generate secondary flows, enhance mixing and thin the thermal boundary layer (TBL), thereby improving convective heat transfer. Converging pipes, whose cross-sectional area decreases along the flow direction, are also effective because they enhance advective heat transfer occurring in the direction of flow. These pipes are widely used due to their ease of fabrication, low maintenance requirements, and high convective heat transfer performance. Improved heat transfer performance is often accompanied by an increase in pressure drops (Zahran *et al*., 2022; Al-Obaidi, 2024). Several studies have experimentally and numerically examined heat transfer regimes in corrugated and converging pipes using various fluids. Dizaji *et al.* (2015) evaluated pressure drop and turbulent CHTP of distilled water flowing through various corrugated pipe shapes (convex and smooth, convex and convex, convex and concave) in a double-pipe heat exchanger using experimental methods. They analysed how different corrugation profiles affected pressure drop and Nusselt number and found that the convex and smooth configuration increased both the pressure drop and the Nusselt number.

Chen *et al.* (2019) investigated the convective heat transfer performance (CHTP) and pressure drop of a heat exchanger equipped with an asymmetrical outward convex corrugated tube (ACT) using both experimental and numerical approaches. They reported that increasing the nondimensionalized fillet radius (r/l) enhanced both the pressure drop and the Nusselt number. Qingchan *et al.* (2021) numerically studied heat transfer in a heat exchanger with sinusoidal plate channels under a turbulent flow regime. They found that a phase shift angle of 324° yielded optimal heat transfer performance. Al-Obaidi (2022) numerically evaluated the hydrothermal performance of distilled water flowing in a laminar regime within a corrugated pipe. The study demonstrated that increasing the number of corrugated rings enhanced both the pressure drop and the Nusselt number, as these rings promoted fluid mixing near the thermal boundary layer, thereby improving thermal performance. Nashee (2023) examined fluid flow and heat transfer in a corrugated channel, analysing the effects of different corrugation orientations (triangular, sinusoidal, square). The results indicated that triangular corrugations provided the best thermal performance but increased the pressure drop.

Liao and Lian (2023) compared a simple corrugated tube (SCT) with a compound corrugated tube (CCT) and found that CCT provides more effective fluid mixing near the walls, resulting in enhanced heat transfer. Zhai *et al.* (2024) numerically investigated the influence of corrugation height, corrugation width, and Reynolds number (4000–12000) on thermal performance. Their results showed that increasing the corrugation height raises turbulent kinetic energy (TKE), vortex formation, and the friction factor, while decreasing the Nusselt number. Conversely, a larger corrugation width produces the opposite effects. Therefore, for this specific pipe design, a larger corrugation width combined with a smaller overall pipe diameter appears to be the most advantageous configuration.

A study on converging pipes was conducted by Hamediani (2020), who examined the impact of operational and geometrical parameters on the heat transfer performance of nanofluids in a convergent-divergent tube under turbulent conditions. The study considered various cone wall diameters, cone pitches, and cone heights, using two different water-based nanofluids, namely water/Al_2O_3 and water/CuO. Their results indicated that water/Al_2O_3 exhibits superior thermal performance compared to the other nanofluids. Zada *et al.* (2024) studied the heat transfer performance of engine oil flowing with hybrid nanoparticles in a convergent-divergent channel. The study examined different velocity profiles under varying Hartmann numbers. In the convergent section, a higher porosity parameter resulted in an increased temperature field. Kaood *et al.* (2024) examined the hydrothermal and entropy generation performance of convergent tubes with various dimple shapes under turbulent flow conditions. The results revealed that the stepped conical convergent tube achieved the highest mean thermal enhancement factor, with a 7.81% improvement compared to a smooth pipe.

Laila and Marwat (2021) adopted a numerical approach to evaluate the CHTP of a nanofluid flowing through a rectangular converging-diverging channel. The effects of Reynolds number and nanoparticle

volume fraction on the average Nusselt number and pressure drop were analysed. The results showed that increasing the Reynolds number and nanoparticle concentration enhanced thermal performance. Iweka and Fadodun (2021) examined the heat transfer performance of an AlO_3/H_2O nanofluid flowing in a Bessel-like converging pipe under laminar flow conditions. The authors investigated the effects of nanoparticle volume fraction $(0 \leq \varphi \leq 3\%)$, convergence index $(0 \leq \theta \leq 3)$, and Reynolds number $(300 \leq Re \leq 1200)$ on the average Nusselt number and drop in pressure. The outcomes revealed that increasing the convergence index, volume fraction, and Reynolds number enhanced both the convective thermal performance and pressure drop. Furthermore, the performance evaluation criterion (PEC) of Bessel-like converging pipes improved as the Reynolds number decreased. Based on the previous literature, few studies have combined two different passive enhancement techniques, particularly corrugated and converging pipes, to achieve improved thermal efficiency. Therefore, the present study aimed to integrate corrugation and convergence in a single-pipe configuration, to investigate how corrugation amplitude and Reynolds number affect the thermal performance of distilled water flowing through corrugated converging pipes, and to examine the effect of Reynolds number on the Poiseuille number and PEC.

2. Methodology

2.1 Description of the Physical Model of the Pipe

The study examined the heat transfer performance of distilled water passing through an outwardly corrugated converging pipe in the turbulent regime. Figure 1(a) illustrates the three-dimensional (3D) pipe used in this work. The examined pipe length was constructed to vary the size of the inlet to outlet diameter while keeping the surface area and the total sum of both the inlet and outlet diameters constant. Thus, the 3D was reduced to a 2D in order to minimise the cost and computational time. Figures 1(b) and 1(c) show the 2D axisymmetric geometries. The investigation was conducted under a fully developed turbulent flow regime. The geometrical dimensions of the corrugated pipes and the diameter ratio (DR) of the converging pipes are presented in Tables 1 and 2, respectively.

Table 1: The geometrical dimension of the corrugated pipes

Parameter	Values (mm)
Corrugation amplitude $\left(\frac{e}{D}\right)$	0.2, 0.3, & 0.4
Corrugation width $\left(\frac{w}{D}\right)$	0.02
Trough between two corrugations $\left(\frac{p-w}{D}\right)$	0.6
Length of the Pipe (L)	0.4
Diameter of the Pipe (D)	0.03 m

Table 2: The Diameter ratio (DR) used for the study

$\boldsymbol{DR = \frac{D_{in}}{D_{out}}}$	$\boldsymbol{D_{in}(m)}$	$\boldsymbol{D_{out}(m)}$
1	0.015	0.015
1.2	0.01636	0.01386

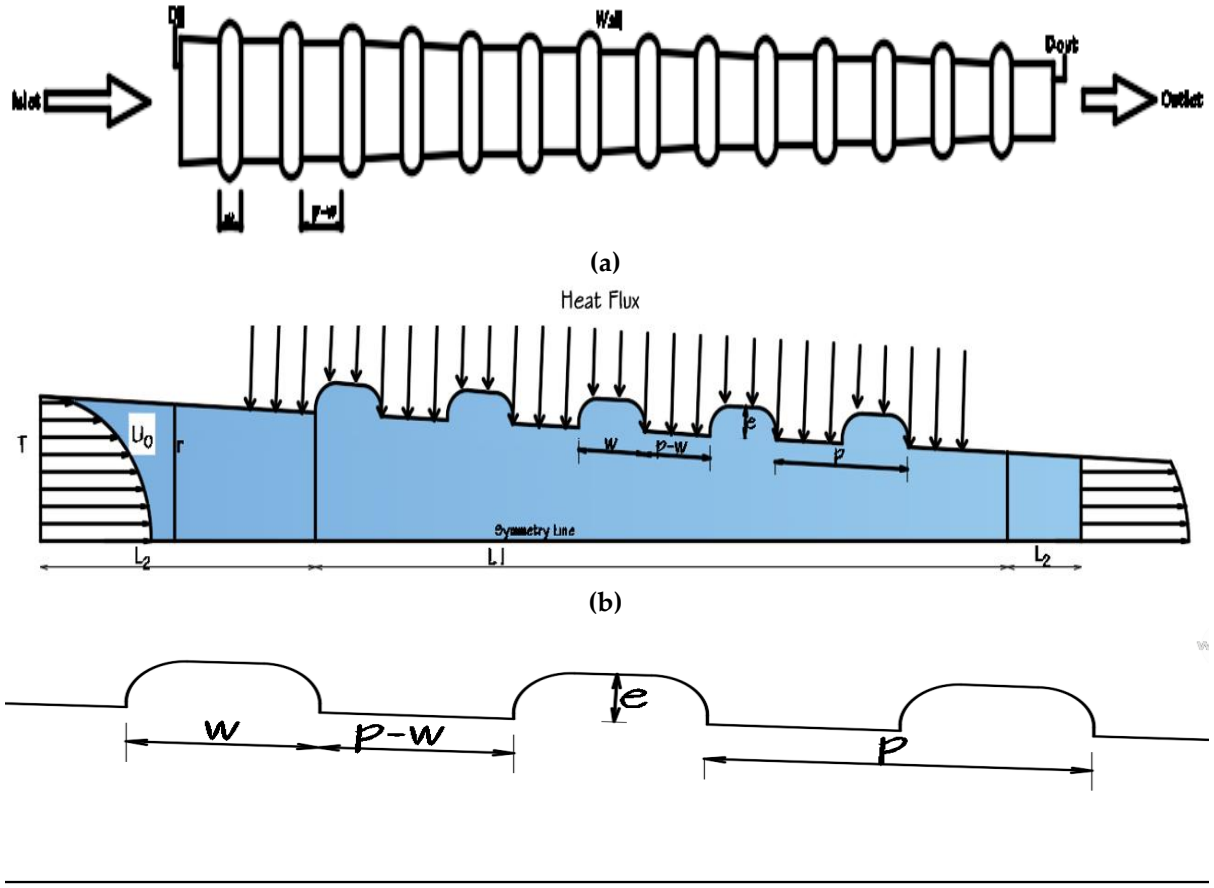

Figure 1: (a) The outwardly Corrugated Converging Pipe (3D geometry), (b) 2D Axisymmetric model of corrugated converging pipe and (c) Description of the Geometric Parameters

The steady state governing equations include the conservation of mass (continuity), momentum (Reynolds-averaged Navier–Stokes), and energy equations, which are expressed as (Abdullah *et al*., 2021; Fadodun *et al*., 2024):

Continuity Equation:

$$\frac{\partial}{\partial x_i}(\rho u_i) = 0 \tag{1}$$

Momentum Equation

$$\frac{\partial}{\partial x_j}(\bar{\rho}\bar{u}_i\bar{u}_j) = -\frac{\partial \bar{p}}{\partial x_i} + \frac{\partial}{\partial x_j}\left[\mu\left(\left(\frac{\partial u_j}{\partial x_i} + \frac{\partial u_i}{\partial x_j}\right) - \frac{2}{3}\frac{\partial u_i}{\partial x_j}\delta_{ij}\right)\right] + \frac{\partial}{\partial x_j}\left(-\rho\overline{\acute{u}_i\acute{u}_j}\right) \tag{2}$$

Energy equation

$$\frac{\partial}{\partial x_i}[u_i(\rho E + P)] = \frac{\partial}{\partial x_j}\left[\left(\lambda + \frac{C_P\mu_t}{Pr_t}\right)\frac{\partial T}{\partial x_j} + u_i(\tau_{ij})_{eff}\right] = 0 \tag{3}$$

The deviatoric stress tensor (τ_{ij}) is expressed as

$$(\tau_{ij})_{eff} = \mu_{eff}\left[\left(\frac{\partial u_j}{\partial x_i} + \frac{\partial u_i}{\partial x_j}\right) - \frac{2}{3}\frac{\partial u_i}{\partial x_j}\delta_{ij}\right] \tag{4}$$

where, $\bar{p}$ is the pressure, u is the velocity, μ is the dynamic viscosity, ρ is the density of the liquid, μ_t is the turbulent viscosity, C_P is the specific heat capacity, E is the total energy, k is the thermal conductivity, T is the temperature, Pr_t is the turbulent Prandtl number, and $\rho\overline{\acute{u}_i\acute{u}_j}$ is the Reynolds tensor stress.

The SST k- ω turbulent model is applicable, since flow separation is expected as a result of the presence of corrugation. This model captures flow separation accurately compared with other RANS models Li *et al*., 2023). The turbulence kinetic energy (k) and the dissipation rate (ω) equations are shown in Equations (5) and (6):

$$\frac{\partial(\rho k u_i)}{\partial x_i} = \frac{\partial}{\partial x_i}\left[\Gamma_k \frac{\partial k}{\partial x_i}\right] + G_k - Y_k \tag{5}$$

$$\frac{\partial(\rho\omega u_i)}{\partial x} = \frac{\partial}{\partial x_i}\left[\Gamma_\omega \frac{\partial \omega}{\partial x_i}\right] + G_\omega - Y_\omega + 2(1-F_1)\rho\sigma_{\omega,2}\frac{1}{\omega}\frac{\partial k}{\partial x_i}\frac{\partial \omega}{\partial x_i} \tag{6}$$

where i and j represent the two coordinates (x and y). The terms G_k and G_ω represent the production of turbulent kinetics due to average velocity gradients and production rates of k and ω. The symbols Y_k and Y_ω represent the turbulent dissipations of k and ω and are written as:

$$Y_\omega = \rho\omega^2\beta_2 \tag{7}$$

$$Y_k = \rho k\omega\beta_1 \tag{8}$$

$$\Gamma_k = \mu + \frac{\mu_t}{\sigma_k} \tag{9}$$

$$\Gamma_\omega = \mu + \frac{\mu_t}{\sigma_\omega} \tag{10}$$

The terms Γ_k and Γ_ω in Eqs. (9) and (10) denote the effective diffusivity of k and ω.

$$\sigma_\omega = \frac{1}{\frac{F_1}{\sigma_{\omega,1}} + \frac{(1-F_1)}{\sigma_{\omega,2}}} \tag{11}$$

The turbulent viscosity (μ_t) is modeled as:

$$\mu_t = \frac{\rho k}{\omega}\frac{1}{\left(\frac{1}{\alpha^*}\frac{SF_2}{\alpha_1\omega}\right)} \tag{12}$$

where the strain rates σ_k and σ_ω are the effective turbulent Prandtl numbers for k and ω, F_1 and F_2 are the blending functions, and α^* is a model constant.

$$\sigma_k = \frac{1}{\frac{F_1}{\sigma_{k,1}} + \frac{(1-F_1)}{\sigma_{k,2}}} \tag{13}$$

$$F_1 = tan(\varphi_1{}^4) \tag{14}$$

$$F_2 = tan(\varphi_2{}^4) \tag{15}$$

where,

$$\varphi_1 = min\left[max\left(\frac{\sqrt{k}}{0.09\omega y^{+}}, \frac{500\mu}{\rho y^{+2}\omega}\right), \frac{4\rho k}{\sigma_{\omega,2} D^{+}{}_{\omega} y^{+2}}\right] \tag{16}$$

$$D^{+}{}_{\omega} = \left[2 \times 10^{-20} \frac{\rho}{\sigma_{\omega,2}\omega} \frac{\partial \omega}{\partial x_j} \frac{\partial k}{\partial x_j}\right] \tag{17}$$

$$\varphi_2 = max\left[\left(\frac{2\sqrt{k}}{0.09\omega y} \frac{500\mu}{\rho y^2 \omega}\right)\right] \tag{18}$$

The SST $k-\omega$ model constants used in this study are $\zeta^* = 1.5$, $\beta_\infty{}^* = 0.09$, $\sigma_k = \sigma_\omega = 2$, $\beta_i = 0.072$, $R_k = 6$, $R_\beta = 8$, $R_\omega = 2.95$, $\alpha_\infty{}^* = 1$, $\propto_\infty = 0.52$, $\sigma_0 = \frac{1}{9}$

Boundary Conditions

Inlet

$u_{x,in} = Prescribed\ velocity,\ u_{r,in} = 0,\ T_{in} = 300K,\ k = \frac{3}{2}(I\ u_{in})^2,\ \ \omega = \frac{c_\mu^{0.75} k^{0.5}}{D_h}$

Outlet

$P_{gauge} = 0,\ \frac{\partial u_x}{\partial x} = 0,\ \frac{\partial u_r}{\partial r} = 0,\ \frac{\partial T}{\partial x} = 0\ \frac{\partial k}{\partial x} = 0,\ \ \frac{\partial \omega}{\partial x} = 0,$

Wall:

No-slip $(u_x = 0, u_r = 0),\ q'' = 5{,}000\ Wm^{-2}$

Symmetry line:

$\left(\frac{\partial u_x}{\partial r} = 0,\ \frac{\partial T}{\partial r} = 0\right)$

The aforementioned governing equations and turbulence models were evaluated via the finite volume method (FVM) in ANSYS Fluent software while considering the boundary conditions stated above.

Thermophysical Properties of Water

In this study, distilled water was used as a working fluid. The thermophysical properties of distilled/H_2O at different temperatures- including density, viscosity, thermal conductivity, and specific heat capacity were experimentally determined and are expressed as follows (Kays and Weigand, 2005; Fadodun and Fadodun, 2024):

$$\rho_f = 330.12 + 5.92T - 1.63 \times 10^{-2}T^2 + 1.33 \times 10^{-5}T^{-3} \tag{19}$$

$$C_P = 10^{-3}(10.01 - 5.14 \times 10^{-2}T + 1.49 \times 10^{-4}T^2 - 1.43 \times 10^{-7}T^3) \tag{20}$$

$$\mu_f = 0.00002414 \times 10^{\left(\frac{247.81}{T-140}\right)} \tag{21}$$

$$k_f = 0.76761 + 7.53211 \times 10^{-3}T - 0.98244 \\ +\times 10^{-5}T^2 \quad (22)$$

Each thermophysical property was evaluated at an inlet temperature (300 K), as the temperature gradient between the inlet and outlet regions is less than 2 K. Therefore, these properties were assumed to remain constant throughout the simulation. Table 3 shows the thermophysical properties employed in this study.

Mesh Generation

A fine mesh is applied near the wall pipe to ensure that the height of the first layer cell lies inside the viscous layer ($y^+ \approx 1$). This was done to accurately apprehend the boundary layer effect. The size of the mesh decreases along the radial direction as depicted in Figure 2. The energy, momentum, and turbulent equations were discretised using a second-order upwind scheme (Javed *et al*., 2023). The semi-implicit method for pressure link equation (SIMPLE) algorithm was adopted to implement pressure – velocity coupling. The discretised equations were solved iteratively, with the convergence criteria set to 10^{-8}, such that:

$$\left|\frac{M^{i+1} - M^i}{M^{i+1}}\right| \leq 10^{-8} \quad (23)$$

where M and i denote field variables and the number of iterations, respectively.

Data Deductions

These terms are applied to analyse the performance of a system. The Reynolds number (Re) is expressed as (Ajeel *et al*., 2019):

$$Re = \frac{\rho u_{in} D_h}{\mu} \quad (24)$$

where ρ, u_{in}, D_h and μ are the fluid's density, the inlet velocity, the hydraulic diameter, and the viscosity of the working fluid, respectively.

The velocity at the inlet was evaluated from the Reynolds number (Re) and expressed as (Ajeel *et al*., 2018):

$$u_{in} = \frac{Re\mu}{\rho D_h} \quad (25)$$

The heat transfer coefficient (h) is expressed as (Kaood *et al*., 2023):

$$h = \frac{q''}{(T_{wall} - T_{bulk})} \quad (26)$$

where, T_{wall} is the temperature of the pipe wall and T_{bulk} is the mean fluid temperature.

The Nusselt number (Nu) is estimated as follows (Safarzadeh *et al*., 2021):

$$Nu = \frac{hD_h}{k} \quad (27)$$

Substituting Eqn. (27) into (28), we obtain:

$$Nu = \frac{q''D_h}{(T_{wall} - T_{bulk})k} \quad (28)$$

where T_{bulk} is calculated by (Zhong *et al*., 2024):

$$T_{bulk} = 0.5(T_{in} + T_{out}) \tag{29}$$

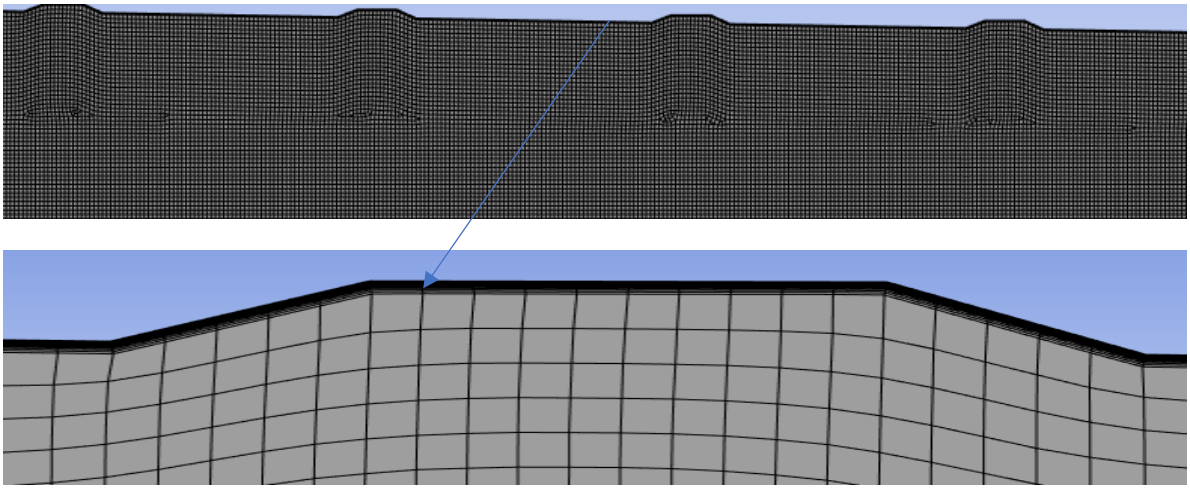

Figure 2: Mesh captured with the Boundary Layer

The Prandtl number is expressed as Cao *et al.* (2021):

$$Pr = \frac{\mu Cp}{k} \tag{30}$$

The friction factor, denoted by f, is given by (Chen *et al*., 2019):

$$f = \frac{2D_h \Delta P}{\rho u^2 L} \tag{31}$$

The Poiseuille number, fRe, is the product of the friction factor and Reynolds number, which is written as:

$$fRe = \frac{2{D_h}^2 \Delta P}{\mu u L} \tag{32}$$

where D_h, $\Delta P, u, \mu$ and L are the hydraulic diameter, pressure drop, velocity of the fluid, viscosity, and pipe length, respectively.

The normalized fRe for modified pipes is expressed as:

$$fRe^N = \frac{fRe_{mod}}{fRe_{str}} \tag{33}$$

where fRe_{mod} and fRe_{str} are the Poiseuille numbers for modified and straight pipes, respectively.

The normalized Nu for the modified pipe expressed as:

$$Nu^N = \frac{Nu_{mod}}{Nu_{str}} \tag{34}$$

where Nu_{mod} and Nu_{str} are the Nusselt numbers in modified and straight pipes, respectively.

The thermal–hydraulic performance evaluation criterion PEC can be evaluated as follows (Al-Obaidi, 2022):

$$PEC = \frac{Nu_{mod}/Nu_{str}}{(f_{mod}/f_{str})^{1/3}} \tag{35}$$

The validation of the Nusselt number (Nu) by Gnielinski is expressed in Eqn. (36), whereas the friction factors (f) by Blasius and Filonenko are shown in Eqns. (37) and (38), respectively (Hu *et al*., 2021).

$$Nu = \frac{\left(f/8\right)(Re - 1000)Pr}{1 + 12.7\left(f/8\right)^{0.5}\left(Pr^{2/3} - 1\right)} \tag{36}$$

$$f = \frac{0.316}{Re^{0.25}} \qquad for\ Re \leq 2 \times 10^4 \tag{37}$$

$$f = (1.82log_{10}Re - 1.64)^{-2} \tag{38}$$

Grid Independence Analysis and Validation

A grid-independence analysis was conducted to determine the optimum number of elements required for accurate results. To perform analysis, various mesh configurations were tested to estimate the average Nusselt number (Nu) of distilled H_2O flowing in an outwardly corrugated converging pipe at $DR = 1.2,\ Re = 4.0 \times 10^4$ and $\frac{e}{D} = 0.03$. Several grid configurations were evaluated, as shown in Table 3. For mesh configurations 97121 and 211659 elements, the corresponding Nu values were 341.25 and 336.711, respectively. The relative error was less than 1.5%. This result shows that the mesh configuration with 97121 elements was sufficient and was therefore selected for the remainder of the study.

For validation purposes, the friction factor (f) and Nusselt number (Nu) of distilled H_2O flowing in a smooth straight pipe were evaluated. The Nu results were compared with the correlations proposed by Gnielinski (1976) in Equation (36), while the f results were compared with the correlations developed by Filonenko (1954) and Blasius (1913) in Equations (37) and (38), respectively. The comparison of Nu is shown in Figure 3, and that of f in Figure 4, showing strong agreement between the numerical results and the established correlations.

Table 3: Grid Independence Analysis

Number of meshes	Nusselt number	Relative error %
25020	361.1412	-
57822	341.2532	5.83
97121	336.7110	1.35
211659	336.7221	0.003

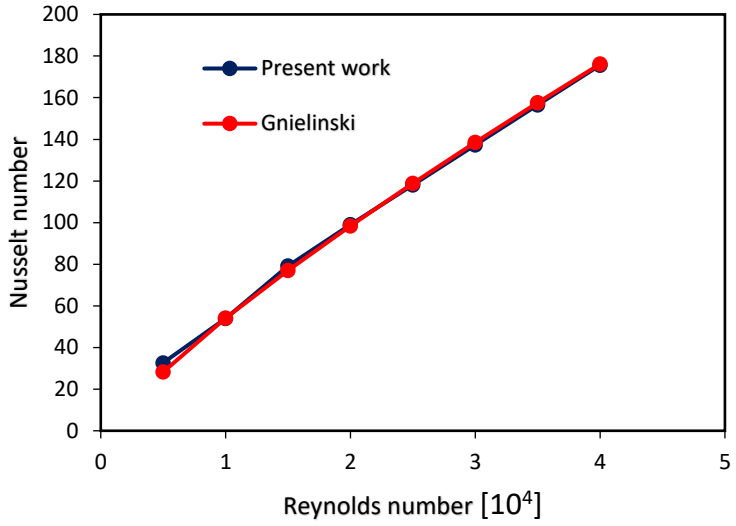

Figure 3: Validation for Nusselt Number

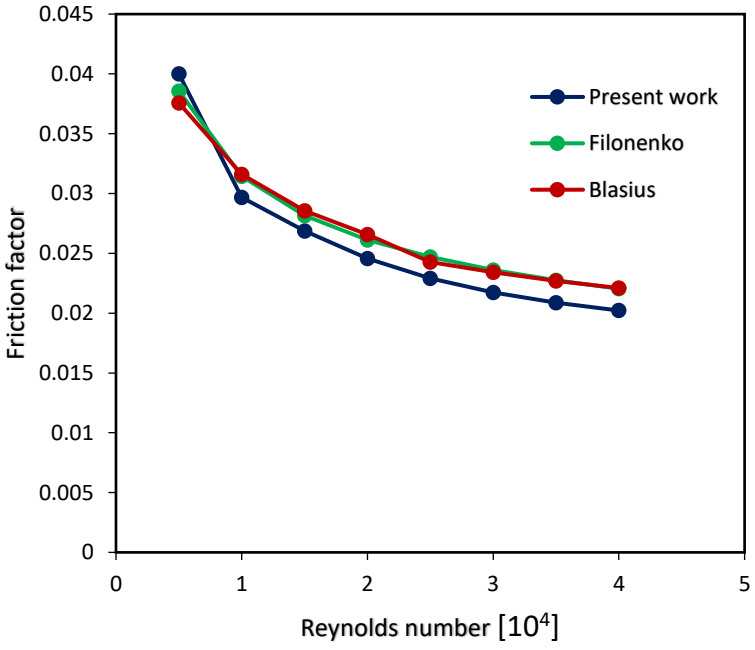

Figure 4: Validation of the Friction Factor

3. Results and Discussion

Convective Heat Transfer Performance (CHTP)

Figure 5 (a) and (b) depict the impact of $\left(\frac{e}{D}\right)$ on the velocity and temperature contours of a straight pipe and the three corrugated converging pipes. At the wall surface, the fluid velocity is zero, confirming that the no-slip condition is appropriately applied. Additionally, recirculation zones were observed within the corrugations due to the adverse pressure gradient (APG). This recirculating flow disrupts

the TBL, causing it to thin and enhancing mixing between the heated fluid near the wall and the unheated fluid in the central region. Furthermore, the flow accelerates in the converging pipe as the diameter ratio (DR) increases, leading to enhanced heat transfer due to increased advection (heat transfer along the flow direction).

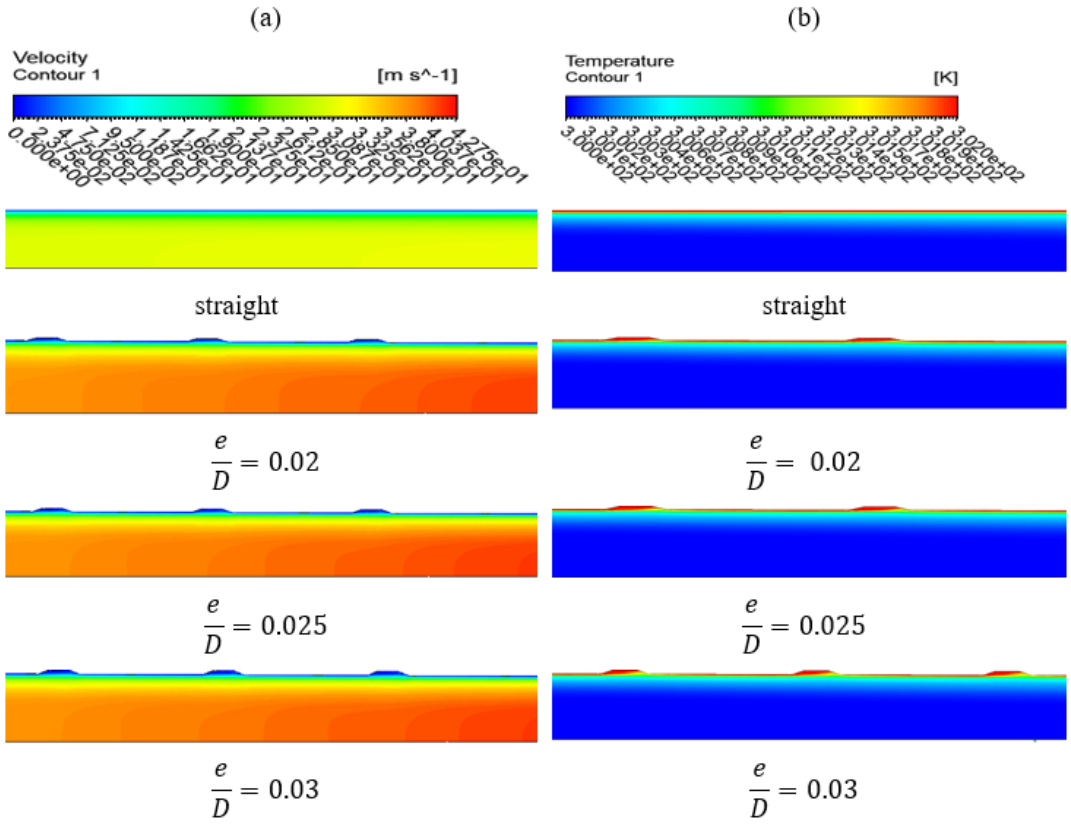

Figure 5: (a) Velocity and (b) Temperature Contours of varying corrugation amplitude of distilled Water Flow in a Straight Smooth Pipe (SP) and Outwardly Corrugated Converging Pipes at $Re = 1.0 \times 10^4$

The velocity contour in the straight pipe remains uniform, validating the assumption that the flow is hydrodynamically fully developed from the inlet section. The TBL in the modified pipe was disrupted compared to that of the smooth pipe due to the presence of corrugations. Furthermore, higher temperatures are observed in the recirculation regions. This is attributed to the low velocity of the recirculating flow which limits heat transfer between the pipe wall and the core fluid region.

Figures 6 (a) and (b) illustrate the impact of $\left(\frac{e}{D}\right)$ on the pressure and turbulent kinetic energy (TKE) contours. The pressure gradually reduces along the flow path for all pipe configurations considered. The adverse pressure gradient (APG) is beneath the corrugations, and its intensity increases as $\left(\frac{e}{D}\right)$ increases. The TKE represents the intensity of mixing between the fluid near the pipe centre and the fluid close to the wall. The TKE is more pronounced in the modified pipe than in the smooth pipe. Its intensity is higher near the pipe surface and decreases toward the core region. This behaviour is expected, as TKE is primarily influenced by velocity fluctuations, which are more significant within the boundary layer along the flow direction. Furthermore, increased TKE enhances the mixing rate between the heated fluid near the wall and the warmer fluid in the pipe core. These two effects lead to an improvement in the CHTP and an increase in the Nusselt number Nu. Consequently, an increase in the Nusselt number Nu.

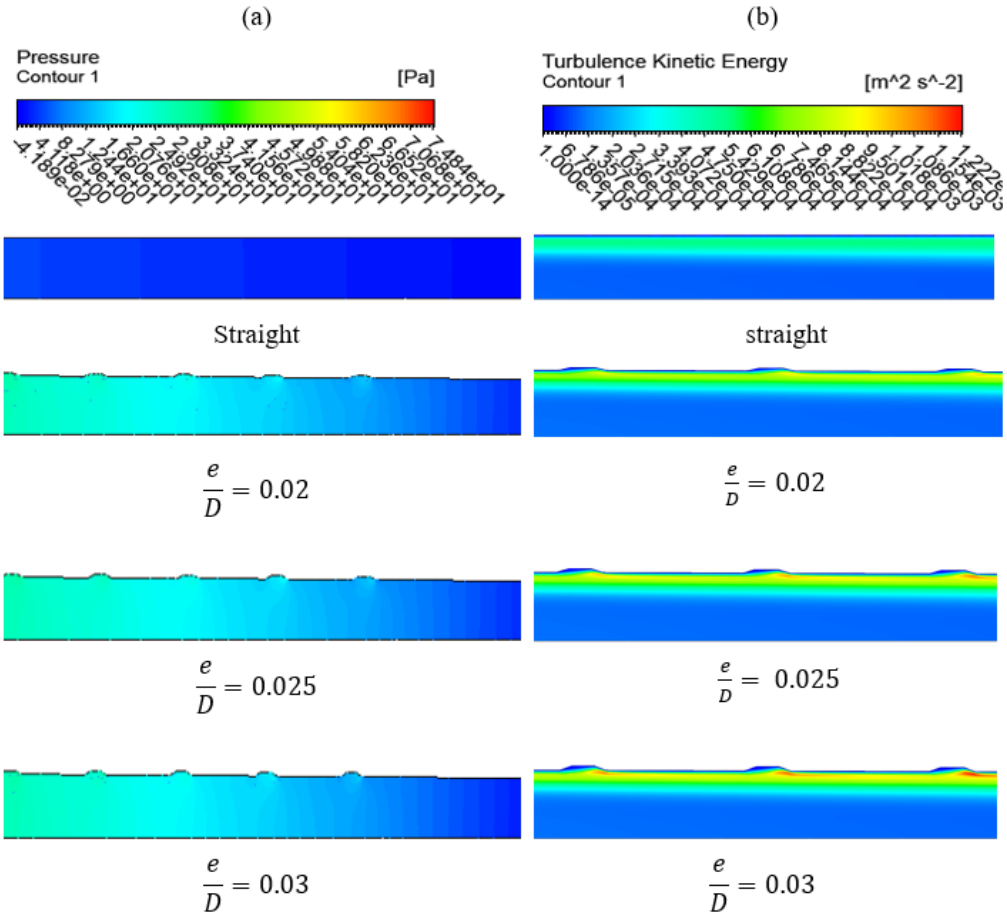

Figure 6: (a) Pressure and (b) Turbulence kinetic energy (TKE) contours of varying corrugation amplitude of distilled water flow in a straight smooth pipe (SP) and outwardly corrugated converging pipes at $Re = 1.0 \times 10^4$

Figure 7a shows the variation of Nu with respect to Re at various $\frac{e}{D}$ values for the modified pipes. The results indicate that Nu is higher in the modified pipes than in the straight pipe because the presence of corrugations induces flow disturbance, which enhances turbulence and mixing near the pipe wall. This reduces the TBL thickness and improves convective heat transfer. Additionally, an increase in Re enhances Nu for all pipe configurations examined. For example, across the investigated Reynolds number range $(0.5 \times 10^4 < Re < 4.0 \times 10^4)$ the values of Nu for $\frac{e}{D} = 0.02, 0.025, 0.03$, at $DR = 1.2$ and $\frac{w}{D} = 0.2$ increase by factors of 6.7, 7.0, and 7.1, respectively. The corresponding value for the straight pipe is 5.8.

The increase in Nu is attributed to the rise in Re, which leads to greater turbulence production and stronger recirculation flow. These two factors enhance mixing and reduce the thermal boundary layer thickness, thereby improving the CHTP and increasing Nu. Considering the impact of $\frac{e}{D}$ on Nu, higher $\frac{e}{D}$ values result in greater Nu. For instance, at $Re = 4.0 \times 10^4, DR = 1.2$ and $\frac{w}{D} = 0.2$, the Nu values for $\frac{e}{D} = (0.02, 0.025 \text{ \& } 0.03)$ are 348.48, 360.69 and 368.78, respectively. This improvement is attributed to the increased flow turbulence and the reduction in TBL thickness, leading to an increase in Nu. In addition, Figure 7b depicts the plot of Nu^G versus Re. The values of Nu^G at $Re = 1.5 \times 10^4$ for $e/D(0.02, 0.025 \text{ \& } 0.03)$ in the modified pipes are 1.36, 1.46 and 1.52, respectively. These results indicate that enhanced convection $(Nu^G > 1)$ is achieved in all corrugated converging pipes.

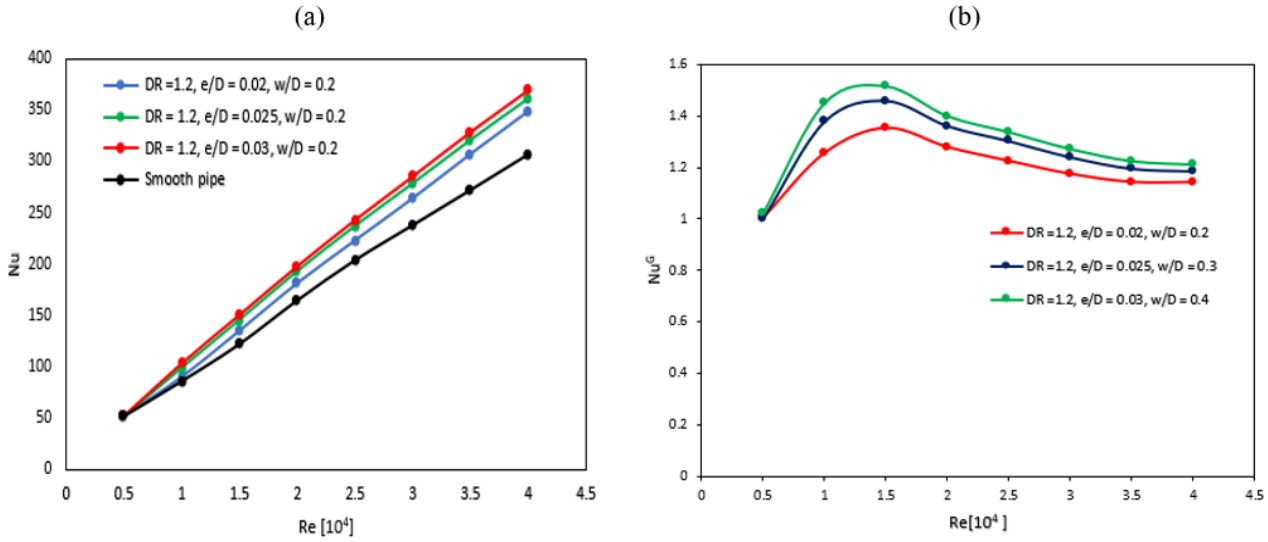

Figure 7: Plots of (a) Nu and (b) Nu^G against Re considering the corrugation amplitude

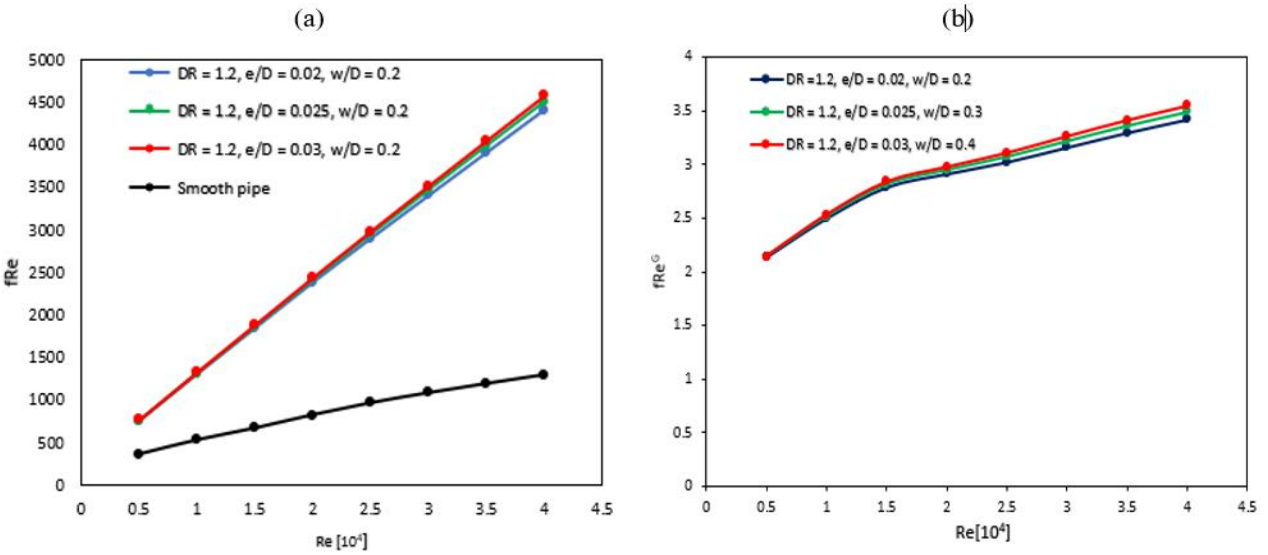

Figure 8: The variation of (a) fRe and (b) fRe^G against Re for different corrugation amplitudes

Figure 8a depicts the variation of fRe with respect to Re at different $\frac{e}{D}$ values for the modified pipes. The outcome revealed that fRe is higher in the modified pipe than in the smooth pipe. Additionally, fRe increases as Re increases. For instance, over the investigated Reynolds number range $(5.0 \times 10^3 < Re < 4.0 \times 10^4)$, the values of fRe for $\frac{e}{D} = 0.02, 0.025$ & 0.03, at $DR = 1.2$ and $\frac{w}{D} = 0.2$ increase by factors of 5.8, 5.9, and 6.1, respectively. The equivalent value for the straight pipe is 4.4. This result is anticipated because higher Re intensifies flow turbulence, increasing flow resistance and, consequently, the required pumping power. Considering the influence of $\frac{e}{D}$ on fRe, as shown in Figure 8a, increasing $\frac{e}{D}$ enhances fRe. For example, at $Re = 4.0 \times 10^4, DR = 1.2$ and $\frac{w}{D} = 0.2$, the values of fRe of $\frac{e}{D} = 0.02, 0.025$ & 0.03 in the corrugated converging pipes are 4407.89, 4502.67, and 4571.15, respectively. This trend is expected because corrugations act as turbulence promoters, and increasing the corrugation amplitude intensifies turbulence leading to an increase in fRe, as discussed earlier. Figure 8b illustrates the variation of fRe^G with respect Re, showing the influence of e/D on fRe^G. It is noticed that increasing both Re and e/D leads to an increase in fRe^G. For example, at $Re = 3.0 \times 10^4$, the values fRe^G in the corrugated converging pipes for e/D (0.02, 0.025, and 0.03) are 3.16, 3.22 and 3.27, respectively. This indicates that increasing e/D results in a higher friction factor in the modified pipes, which makes fluid flow more difficult due to increased resistance.

Figure 9 presents the variation of the performance evaluation criterion (PEC) against the Re at different $\frac{e}{D}$ values for the corrugated converging pipes. The graph shows that PEC decreases as Re increases. For example, at $Re = 5.0 \times 10^3$, $\frac{e}{D} = 0.02$, $DR = 1.2$ and $\frac{w}{D} = 0.2$, the PEC value is 1.38, whereas the corresponding value at $Re = 4.0 \times 10^4$ is 0.99. This trend is expected because increasing Re results to increase in fRe^G and Nu^G. However, the enhancement in fRe^G is significantly greater than that in Nu^G. Considering the influence of $\frac{e}{D}$ on PEC, an increase in $\frac{e}{D}$ improves the PEC. For example, at $Re = 10^4, DR = 1.2$ and $\frac{w}{D} = 0.2$, PEC values for $\frac{e}{D} = (0.02, 0.025$ and $0.3)$ are 1.25, 1.36, and 1.42, respectively. This indicates that the increase in Nu^G with higher $\frac{e}{D}$ value is accompanied by a proportionally moderate increase in fRe^G, thereby enhancing the overall thermal performance.

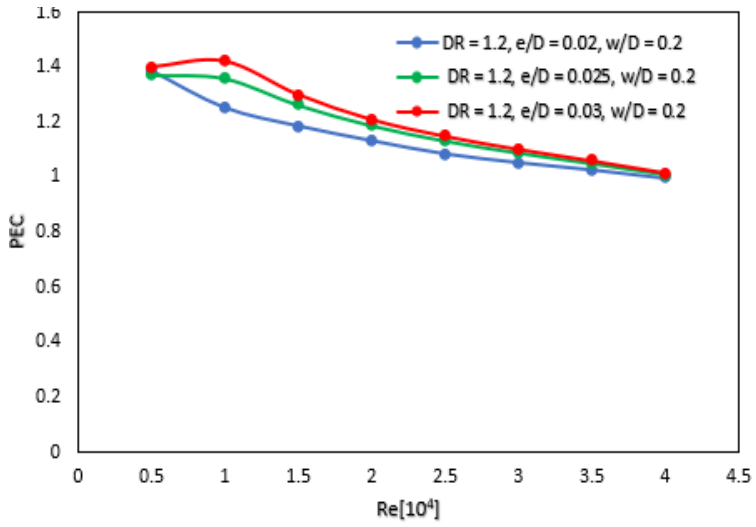

Figure 9: Plot of PEC against Re Considering the Amplitude

Further analysis revealed that, across the Reynolds number range ($5.0 \times 10^3 \leq Re \leq 3.5 \times 10^4$) at $DR = 1.2$ and various corrugation amplitudes ($\frac{e}{D}$), the modified designs exhibit better overall CHTP than smooth straight pipe ($PEC > 1$).

5. Conclusion

This work presents a numerical investigation of the turbulent convective heat transfer performance of distilled/H_2O flowing through a corrugated converging pipe. The finite volume method (FVM) in ANSYS Fluent was used to develop and discretise the governing equations for continuity, momentum (Reynolds-averaged Navier–Stokes), and energy. The SIMPLE algorithm was applied to solve the pressure-velocity coupling. The numerical study examined the effects of the Reynolds number ($0.5 \times 10^4 \leq Re \leq 4.0 \times 10^4$) and corrugation amplitude ($0.02 \leq e/D \leq 0.03$) on the Nusselt and Poiseuille numbers. The results showed that increasing the corrugation amplitude and Reynolds number enhanced convective heat transfer, as indicated by the Nusselt number. This study demonstrates that combining passive enhancement techniques, such as corrugated and converging geometries, improves the heat transfer performance of heat exchangers compared to smooth pipes. These findings may help engineers improve the design of devices such as internal combustion engines, refrigerators, and HVAC systems.

References

Abbas, A. K., & Dhaidan, N. S. (2018). Turbulent forced convection of nanofluids flow in corrugated tubes. In *IOP Conference Series: Materials Science and Engineering*, 433(1), 012054. https://doi.org/10.1088/1757-899X/433/1/012054

Abdullah, M. F., Zulkifli, R., Moria, H., Najm., A. S. Harun, Z., Abdullah, S., Ghopa, A.W., & Sulaiman, N. H. (2021). Assessment of TiO_2 Nanoconcentration and Twin Impingement Jet of Heat Transfer Enhancement- A Statistical Approach: Using Response Surface Methodology. *Energies*, 595(14), 1-29. https://doi.org/10.3390/en14030595

Ajeel, K. R., Salim, W. S., Sopian, K., Yusoff, M. Z., Hasnan, K. Ibrahim, A., & Al-Waeli, H. A. (2019). Turbulent convective heat transfer of silica oxide nanofluid through corrugated channels: An experimental and numerical study. *International Journal of Heat and Mass Transfer*, 145(1), 1-15. https://doi.org/10.1016/j.ijheatmasstransfer.2019.118806

Ajeel, R. K., Salim, W. I., & Hasnan, K. (2018). Thermal performances comparison in various types of trapezoidal corrugated channel using nanofluids, *International Review of Mechanical Engineering* 12(8), 672-683. https://doi.org/10.15866/ireme.v12i8.15114

Al-Daamee, F. Q., & Hamza, N. H. (2024). Numerical investigation of thermal and entropy generation characteristics in a sinusoidal corrugated channel under the influence of sinusoidal wall temperature. *International Journal of Thermofluids*, 22(3), 1-15. https://doi.org/10.1016/j.ijft.2024.100706

Al-Obaidi, A. R. (2022). Investigation on effects of varying geometrical configurations on thermal hydraulics flow in a 3D corrugated pipe. *International Journal of Thermal Sciences*, 171, 107237. https://doi.org/10.1016/j.ijthermalsci.2021.107237

Al-Obaidi, A. R. (2024). Investigation evaluation of thermo-hydraulic flow and heat improvement in a 3D circular corrugated pipe based on response surface method and Taguchi analyses. *Heat and Mass Transfer*, 60(4), 573-597. https://doi.org/10.1007/s00231-024-03456-1

Blasius, H. (1913). Das Aehnlichkeitsgesetz bei Reibungsvorgängen in Flüssigkeiten,Berlin Heidelberg, Berlin, Heidelberg, Heidelberg, *Springer*, 3(1), 1-41. https://doi.org/10.1007/978-3-662-02239-9_1

Calomino, F., Alfonsi, G., Gaudio, R., D'Ippolito, A., Lauria, A., Tafarojnoruz, A., & Artese, S. (2018). Experimental and numerical study of free-surface flows in a corrugated pipe. *Water*, 10(5), 638. https://doi.org/10.3390/w10050638

Cao, Y., Ayed, H., Anqi, A. E., Tutunchian, O., & Dizaji, H. S. (2021). Helical tube-in-tube heat exchanger with corrugated inner tube and corrugated outer tube: experimental and numerical study. *International Journal of Thermal Sciences*, 170(1), 1-13. https://doi.org/10.1016/j.ijthermalsci.2021.107139

Chaurasiya, P. K., Singh, S. K., Jain, P. K., Rajak, U., Verma, T. N., Azad, A. K., & Khan, A. (2023). Heat transfer and friction factor correlations for double pipe heat exchanger with inner and outer corrugation. *Energy Sources, Part A: Recovery, Utilization, and Environmental Effects*, *45*(1), 18-45. https://doi.org/10.1080/15567036.2021.1953635

Chen, X., Han, H. Lee, K. S., Lia, B., & Zhang, Y. (2019). Turbulent heat transfer enhancement in a heat exchanger using asymmetrical outward convex corrugated tubes. *Nuclear Engineering and Design*, 350, 78-89. https://doi.org/10.1016/j.nucengdes.2019.05.001

Corcoles, J. I., Moya-Rico, J. D., Molina, A. E., & Almendros-Ibanez. J.A. (2020). Numerical and experimental study of the heat transfer process in a double pipe heat exchanger with inner corrugated tubes. *International Journal of Thermal Sciences*, 158(1), 1-12. https://doi.org/10.1016/j.ijthermalsci.2020.106526

Dizaji, H. S., & Jafarmadar, S. (2015). Experiments on New Arrangements of Convex and Concave Corrugated Tubes through a Double-pipe Heat Exchanger. *A Journal of Thermal Energy Generation, Transport, Storage and Conversion*, 29(5), 577-592. https://doi.org/10.1080/08916152.2015.1046015

Fadodun, O.G., Fadodun, O. O., & Kaood, A. (2024). Numerical investigation of hydrothermal performance and entropy production rates of rGO-CO_3O_4/H_2O hybrid nanofluid in wavy channels using discrete phase model. *International Journal of Thermal Sciences*, 19(1), 1-17. https://doi.org/10.1016/j.ijthermalsci.2023.108724

Fadodun, O.O., & Fadodun, O.G. (2024). Hydrothermal performance and irreversibility production of distilled H_2O flowing in outwardly corrugated converging pipes. *International Journal of Computation and Methodology*, 2(1), 1-20. https://doi.org/10.1080/10407782.2024.2379614

Filonenko, G. K. (1954). Hydraulic resistance of pipes with smooth walls. *Journal of Engineering Physics*, 26(8), 1009-1013.

Gnielinski, V. (2013). "Corrigendum to "On heat transfer in tubes. *International Journal of Heat and Mass Transfer*, 63, 134-140.

Hamediani, F. A., Ajarostaghi, S. S., & Hosseini, S. A. (2020). Numerical evaluation of the effect of geometrical and operational parameters on thermal performance of nanofluid flow in convergent-divergent tube. *Journal of Thermal Analysis & Calorimetry*, 140(3), 1483. https://doi.org/10.1007/s10973-019-08765-w

Hu, Q., Yuan, K., Peng, W., Zhao, G., & Wang, J. (2021). A numerical study of heat transfer enhancement by helically corrugated tubes in the intermediate heat exchanger of a very-high temperature gas-cooled reactor. *Nuclear Engineering and Design*, 380, 111275. https://doi.org/10.1016/j.nucengdes.2021.111275

Iweka, S. I., & Fadodun, O. G. (2021). Numerical modelling of heat transfer in Al_2O_3/H_2O nanofluid flowing through a Bessel-like converging pipe. *Journal archives of thermodynamics*, 42(2), 121-153. https://doi.org/10.24425/ather.2021.137557

Javed, S., Deb, N., & Saha, S. (2023). Natural convection and entropy generation inside a square chamber divided by a corrugated porous partition. *Journal Results in Engineering*,18(1), 1-14. https://doi.org/10.1016/j.rineng.2023.101053

Kaood, A., Aboumagd, A., & El-Degwy, A. (2023). Entropy generation analysis of turbulent flow in conical tubes with dimples: a numerical study. *Journal of Thermal Analysis and Calorimetry*, 148(1), 5667-5685. https://doi.org/10.1007/s10973-023-12127-y

Kaood, A., ElDegwy, A., & Aboulmagd, A., (2024). Hydrothermal and entropy generation performance of convergent tubes with various dimple shapes. *International Journal of Thermal Sciences*, 197,108842. https://doi.org/10.1016/j.ijthermalsci.2023.108842

Kays, W. M., Crawford, M. E., & Weigand, B. (2005). Convective heat and mass transfer. *Boston: McGraw-Hill Higher Education*, 76(1), 81-89.

Laila, R., & Marwat, D. N. (2021). Nanofluid flow in a converging and diverging channel of rectangular and heated walls. *Ain Shams Engineering Journal*, 12(4), 4023-4035. https://doi.org/10.1016/j.asej.2021.02.030

Li, X., Liu, S., Mo, X., Sun, Z., Tian, G., Xin, Y., & Zhu, D. (2023). Investigation on Convection Heat Transfer Augment in Spirally Corrugated Pipe. *Energies*, 16(3), 1063- 1072. https://doi.org/10.3390/en16031063

Liao, W., & Lian, S (2023). Effect of compound corrugation on heat transfer performance of corrugated tube. *International Journal of Thermal Sciences*, 185, 108036. https://doi.org/10.1016/j.ijthermalsci.2022.108036

Liao, W., Luo, Y., & Chen, T. (2021). Thermal- hydraulic performance analysis of outward convex corrugated tubes based on skewness and kurtosis. *International Journal of Thermal Sciences*, 165(1), 1-13. https://doi.org/10.1016/j.ijthermalsci.2021.106970

Liu, C., Zhang, S., Zheng, C., Wang, W., Wang, Y., Liu, Z., & Chen, Z. (2024). Heat transfer enhancement characteristics of sinusoidal corrugated tubes fabricated via laser powder bed fusion. *Case Studies in Thermal Engineering*, 60, 104722. https://doi.org/10.1016/j.csite.2024.104722

Nashee, S. R. (2023). Numerical Study for Fluid and Heat Transfer Characteristics in a Corrugating Channel. *International Journal of Heat and Technology*, 41(2), 392-398. https://doi.org/10.18280/ijht.410213

Peng, H., Huang, L., Tian, R., Lv, X., Yuan, J., Liu, Y., and Xu, S. (2025). Study on flow and heat transfer characteristics of LNG in flexible corrugated pipes. *International Journal of Thermal Sciences*, 217, 110089. https://doi.org/10.1016/j.ijthermalsci.2025.110089

Qin, S. Y., Xiao, H., Xiao, Y., Liu, P., Zhou, F. Y., Liu, W., Liu, Z. C., & Shan, F. (2020). Experimental Investigation of the coherent structures in a spirally corrugated pipe. *International Journal of Heat and Fluid Flow,* 84(1), 1-10. https://doi.org/10.1016/j.ijheatfluidflow.2020.108601

Qingchan, M., Yanxia, Y., & Yuqing, Z. (2021). Thermal performance optimization of heat exchanger with mixed cross-corrugated sinusoidal plate channels. *Applied Thermal Engineering*, 195(2), 1-8. https://doi.org/10.1016/j.applthermaleng.2021.117138

Safarzadeh, S. Niknam-Azodi, M., Aldaghi, A., Taheri, A., Passandideh-Fard, M., & Mohammadi, M. (2021). Energy and entropy generation analyses of a nanofluid-based helically coiled pipe under a constant magnetic field using smooth and micro-fin pipes: Experimental study and prediction via ANFIS model. *Journal of Communications in Heat and Mass Transfer*, 126(1), 1-13. https://doi.org/10.1016/j.icheatmasstransfer.2021.105405

Shuvo, M. S., Ruvo, T. H., & Saha, S. (2023). Characteristics of turbulent forced convective nanofluid flow and heat transfer in a 2D axisymmetric corrugated pipe. *Thermal Science and Engineering Progress*, *41*, 101838. https://doi.org/10.1016/j.tsep.2023.101838

Zada, L., Ullah, I., Alqahtani, A. M., Nawaz, R., Khan, H., & Alam, K. (2024). Enhancing energy efficiency and heat transfer performance of engine oil flow through hybrid nanoparticles in convergent/divergent channel. *Results in Engineering*, *22*, 102027. https://doi.org/10.1016/j.rineng.2024.102027

Zahran, S., Sultan, A. A., Bekheit, M., & Elmarghany, M. R. (2022). Heat transfer augmentation through rectangular cross section duct with one corrugated surface: An experimental and numerical study. *Case Studies in Thermal Engineering*, *36*, 102252. https://doi.org/10.1016/j.csite.2022.102252

Zhai, H., Gao, S., Zhang, W., Song, Y., Gong, X., Wang, D., & Lu, Q. (2024). The influence of corrugated pipes parameters on heat transfer characteristics. *Thermal Science*, *28*(1 Part A), 257-267. https://doi.org/10.2298/TSCI230709231Z

Zhang, L., Xiong, W., Zheng, J., Liang, Z., & Xie, S. (2021). Numerical analysis of heat transfer enhancement and flow characteristics inside cross-combined ellipsoidal dimple tubes. *Case Studies in Thermal Engineering*, *25*, 100937. https://doi.org/10.1016/j.csite.2021.100937

Zheng, Z., Huang, X., & Jiang, Z. (2023). Thermal performance and heat transfer reliability analysis in helically corrugated helical tube. *International Journal of Thermal Sciences*, *183*, 107849. https://doi.org/10.1016/j.ijthermalsci.2022.107849

Zhong, Y., Song, Y., Zhao, L., Mi, F., Zhao, J., & Zhu, X. (2024). Large eddy simulation of flow and heat transfer performance in periodically inward corrugated tubes. *International Journal of Thermal Sciences*, 199, 108938. https://doi.org/10.1016/j.ijthermalsci.2024.108938

Funding
Not applicable.

Institutional Review Board Statement
Not applicable.

Informed Consent Statement
Not applicable.

Acknowledgements
Not applicable.

Conflict of Interest
The author declared no conflict of interest in the manuscript.

Authors' Declaration
The author(s) hereby declare that the work presented in this article is original and that any liability for claims relating to the content of this article will be borne by them.

Author Contributions
Conceptualization – T.B.F., A.A.A; Design – T.B.F, A.A.A.; Supervision – A.A.A.; Resources – T.B.F., A.J.A.; Materials – T.B.F., A.J.A.; Data Collection – T.B.F., A.J.A.; Analysis – T.B.F.; Literature Search – T.B.F; Writing – T.B.F., A.J.A.; Critical Reviews – T.B.F., A.A.A., A.J.A.

Cite article as:

Fasiku, T.B., Amosun, A.A. & Awodunmila, A.J. (2026). Numerical Investigation of Turbulent Convective Heat Transfer of Distilled Water Flowing in Corrugated Converging Pipes. *Ajayi Crowther Journal of Pure and Applied Sciences, 5*(1), 11–27. https://doi.org/10.56534/acjpas.2026.v5.i1.193